

Supporting Information for
Unraveling Luminescence Mechanisms in Zero-Dimensional Halide
Perovskites

Dan Han^{1,2,3,†} Hongliang Shi^{4,†*} Wenmei Ming³, Chenkun Zhou⁵, Biwu Ma⁵, Bayrammurad
Saparov,⁶ Ying-Zhong Ma³, Shiyong Chen², and Mao-Hua Du^{3*}

¹Key Laboratory of Polar Materials and Devices (Ministry of Education) and ²Department
of Physics, East China Normal University, Shanghai 200241, China

³Materials Science and Technology Division, Oak Ridge National Laboratory, Oak Ridge, TN
37831, USA

⁴Key Laboratory of Micro-Nano Measurement-Manipulation and Physics (Ministry of
Education), Department of Physics, Beihang University, Beijing 100191, China

⁵Department of Chemical and Biomedical Engineering, FAMU-FSU College of Engineering,
Tallahassee, FL 32310, USA

⁶Department of Chemistry and Biochemistry, University of Oklahoma, 101 Stephenson Parkway,
Norman, OK 73019, USA

Keywords: Halide perovskite; $(\text{C}_4\text{N}_2\text{H}_{14}\text{X})_4\text{SnX}_6$; Cs_4PbBr_6 ; Luminescence; DFT calculations

[†]Both authors contributed equally to this work.

*Corresponding Author: Mao-Hua Du (mhdu@ornl.gov); Hongliang Shi (hlshi@buaa.edu.cn)

S1. Computational Details

All calculations were based on density functional theory (DFT) implemented in the VASP code.¹ The interaction between ions and electrons was described by projector augmented wave method.² The kinetic energy cutoff of 400 eV for the plane-wave basis was used for all calculations except the dielectric constant calculations, in which a higher energy cutoff of 520 eV was used. Experimental lattice parameters of $(\text{C}_4\text{N}_2\text{H}_{14}\text{Br})_4\text{SnBr}_6$ [space group $P-1$ (# 2); $a = 10.2070 \text{ \AA}$, $b = 10.6944 \text{ \AA}$, $c = 18.5996 \text{ \AA}$, $\alpha = 94.043^\circ$, $\beta = 102.847^\circ$, $\gamma = 97.904^\circ$], $(\text{C}_4\text{N}_2\text{H}_{14}\text{I})_4\text{SnI}_6$ [space group $P-1$ (# 2); $a = 10.7464 \text{ \AA}$, $b = 10.8924 \text{ \AA}$, $c = 11.1796 \text{ \AA}$, $\alpha = 94.043^\circ$, $\beta = 102.847^\circ$, $\gamma = 97.904^\circ$]³ and Cs_4PbBr_6 [space group $R-3C$ (#167); $a = b = c = 9.8019 \text{ \AA}$, $\alpha = \beta = \gamma = 88.8480^\circ$]⁴ were used while the atomic positions were fully relaxed until the residual forces were less than 0.02 eV/ \AA .

S2 Electronic Structure

The calculated band gaps of $(\text{C}_4\text{N}_2\text{H}_{14}\text{Br})_4\text{SnBr}_6$, $(\text{C}_4\text{N}_2\text{H}_{14}\text{I})_4\text{SnI}_6$, and Cs_4PbBr_6 (as shown in the band structures in Figure 2) are 3.46 eV, 2.90 eV, and 3.19 eV, respectively, at the PBE level, which are underestimated due to the well-known band gap error in PBE calculations; they are increased substantially by including Fock exchange in hybrid PBE0⁵ calculations (Table S1). $(\text{C}_4\text{N}_2\text{H}_{14}\text{X})_4\text{SnX}_6$ ($X = \text{Br}, \text{I}$) have direct band gaps at the Y point. The band gap of Cs_4PbBr_6 is indirect; the VBM is at the Γ point while the CBM is located near the Z point along the Γ -Z direction. Due to the strong charge localization in 0D metal halides, the optical emission and the onset of the optical absorption are due to strongly localized excitons instead of the band-to-band optical transition. Thus, the calculated band gaps should not be compared with the experimentally measured optical absorption and excitation energies^{3, 6}.

Table S1. Band gaps (in eV) of $(\text{C}_4\text{N}_2\text{H}_{14}\text{Br})_4\text{SnBr}_6$, $(\text{C}_4\text{N}_2\text{H}_{14}\text{I})_4\text{SnI}_6$, and Cs_4PbBr_6 calculated using PBE and hybrid PBE0 methods. Spin-orbit coupling is included in the calculations for Cs_4PbBr_6 only.

	PBE	PBE0
$(\text{C}_4\text{N}_2\text{H}_{14}\text{Br})_4\text{SnBr}_6$	3.46	5.10
$(\text{C}_4\text{N}_2\text{H}_{14}\text{I})_4\text{SnI}_6$	2.90	4.43
Cs_4PbBr_6	3.19	4.80

S3 Dielectric Constant

Calculated dielectric constants of 0D halide perovskites $(\text{C}_4\text{N}_2\text{H}_{14}\text{Br})_4\text{SnBr}_6$, $(\text{C}_4\text{N}_2\text{H}_{14}\text{I})_4\text{SnI}_6$, and Cs_4PbBr_6 as well as those of 3D halide perovskites $\text{CH}_3\text{NH}_3\text{SnBr}_3$, $\text{CH}_3\text{NH}_3\text{SnI}_3$, and CsSnBr_3 are shown in Table S2. They were calculated based on experimental lattice parameters, which are shown in Sec. S1 for $(\text{C}_4\text{N}_2\text{H}_{14}\text{Br})_4\text{SnBr}_6$, $(\text{C}_4\text{N}_2\text{H}_{14}\text{I})_4\text{SnI}_6$, and Cs_4PbBr_6 , and are taken from References ⁷ and ⁸ and ⁹ for $\text{CH}_3\text{NH}_3\text{SnBr}_3$, $\text{CH}_3\text{NH}_3\text{SnI}_3$, and CsSnBr_3 , respectively.

The main difference in the dielectric constant between the 0D and the 3D compounds is the ionic contribution as shown in Table S2. The mixed ionic-covalent character of the 3D halides that contain ns^2 cations (which has outer electron configuration of ns^2 such as Pb^{2+} and Sn^{2+}) causes strong lattice polarization in response to the electric field, which leads to enhanced Born effective charges and large static dielectric constant (dominated by the ionic contribution).¹⁰⁻¹² This effect diminishes in 0D halide perovskites due to the reduced concentration of the ns^2 cation and the reduced Born effective charges. The lack of the long-range lattice polarization in 0D halide perovskites lowers the Born charges. This is evidenced in Table S3, where the Born charges of 0D Cs_4PbBr_6 are compared with those of 3D CsPbBr_3 . These two inorganic compounds are chosen because both have only one inequivalent Pb and Br sites, which make the comparison simple. The results in Table S3 show that the Born charges of both Pb and Br ions in Cs_4PbBr_6 and CsPbBr_3 are enhanced compared to their nominal ionic charges (which are +2 for Pb and -1 for Br); but the Born charges in 0D Cs_4PbBr_6 are significantly lower than those in 3D CsPbBr_3 .

Table S2. Calculated static dielectric constants ϵ_{st} [including the electronic (ϵ_{∞}) and the ionic (ϵ_{ion}) contributions] of $(C_4N_2H_{14}Br)_4SnBr_6$, $(C_4N_2H_{14}I)_4SnI_6$, Cs_4PbBr_6 , $CH_3NH_3SnBr_3$, $CH_3NH_3SnI_3$, and $CsSnBr_3$ at their room-temperature phases. Note that these are traces of the dielectric tensors.

	ϵ_{∞}	ϵ_{ion}	ϵ_{st}
$(C_4N_2H_{14}Br)_4SnBr_6$	3.0	8.9	11.9
$(C_4N_2H_{14}I)_4SnI_6$	3.3	4.4	7.7
Cs_4PbBr_6	3.1	4.6	7.7
$CH_3NH_3SnBr_3$	4.7	27.3	32.0
$CH_3NH_3SnI_3$	5.6	23.9	29.5
$CsPbBr_3$	4.6	14.6	19.2

Table S3. Calculated Born effective charge tensors for Pb and Br in Cs_4PbBr_6 and $CsPbBr_3$.

	Atom Type	Wyckoff position	Born effective charge tensor
Cs_4PbBr_6	Pb	6b	$\begin{pmatrix} 2.960 & 0.096 & -0.004 \\ -0.003 & 2.958 & 0.096 \\ 0.096 & -0.006 & 2.956 \end{pmatrix}$
	Br	36f	$\begin{pmatrix} -1.939 & -0.269 & 0.167 \\ -0.308 & -1.076 & 0.048 \\ 0.223 & 0.016 & -1.038 \end{pmatrix}$
$CsPbBr_3$	Pb	6b	$\begin{pmatrix} 3.922 & -0.441 & 0.493 \\ -0.003 & 3.920 & -0.000 \\ -0.445 & -0.005 & 3.999 \end{pmatrix}$
	Br	36f	$\begin{pmatrix} -0.807 & -0.020 & 0.0 \\ 0.059 & -0.719 & 0.0 \\ 0.0 & 0.0 & -4.218 \end{pmatrix}$

S4. Exciton Trapping at Halogen Vacancies

To understand exciton trapping at halogen vacancies, we studied all the symmetrically inequivalent halogen vacancies in all three 0D halide perovskites studied here. The results show that the extremely narrow conduction band exposes the metal ion dangling bond (DB) inside the band gap. Taking V_{Br}^+ in $(\text{C}_4\text{N}_2\text{H}_{14}\text{Br})_4\text{SnBr}_6$ as an example, the DOS of the most stable V_{Br}^+ (which is adjacent to a Sn ion) is shown in Figure S3. The empty V_{Br}^+ defect level (Sn-5p DB level) is deep inside the band gap. When the exciton is trapped at V_{Br}^+ , the electron occupies the Sn-5p DB while the hole resides in the Sn-5s-Br-4p hybridized orbital on the SnBr_4 plane which is approximately perpendicular to the Sn-5p DB (Figure S4). As a result, one Sn-Br bond is elongated due to the electron excitation and four other Sn-Br bonds are shortened due to the hole-enhanced Coulomb attraction. The exciton trapping at halogen vacancies in $(\text{C}_4\text{N}_2\text{H}_{14}\text{I})_4\text{SnI}_6$ and Cs_4PbBr_6 invoke similar structural distortion.

S5. Discussion of Experimentally Measured Optical Properties in Green-Emitting Cs_4PbBr_6

The excitation and the emission energies (2.3 eV – 2.4 eV), the narrow emission band (15 nm – 24 nm)¹³⁻¹⁷, and the fast PL decay (a few to a few tens of ns)¹³⁻¹⁷ observed in green-emitting Cs_4PbBr_6 all agree well with those observed in CsPbBr_3 .^{18, 19} The measured band gap of green-emitting Cs_4PbBr_6 is likely the band gap of trace CsPbBr_3 in Cs_4PbBr_6 . The small band gap difference between bulk CsPbBr_3 and green-emitting Cs_4PbBr_6 (a few meV)²⁰ could be due to the strained CsPbBr_3 inclusion within the matrix of Cs_4PbBr_6 . Tensile strain in CsPbBr_3 should increase the band gap because it is known that thermal expansion of CsPbBr_3 increases the band gap¹⁸ due to the antibonding nature of the VBM²¹.

A significant exciton binding energy (~ 353 meV¹⁴; 303.9 meV²²; 222 meV¹³; 159 meV¹⁶) was obtained in green-emitting Cs_4PbBr_6 through the temperature-dependent PL measurement and was used as an evidence of intrinsic luminescence from Cs_4PbBr_6 since the exciton binding energy in CsPbBr_3 is much smaller (~ 40 meV).¹³ However, the measured significant exciton binding energy does not reconcile with the above-band-gap emission.¹⁴ Also, our calculations shows a substantially larger exciton binding energy of 1.25 eV (relative to free excitons) in Cs_4PbBr_6 (Table 1). The excitation energies used in temperature-dependent PL measurements [i.e., 2.62 eV (473 nm)^{14, 16}, 3.27 eV (380 nm)²², and 3.40 eV (365 nm)²²] are in fact below the

calculated band gap of 4.8 eV and the calculated and measured excitonic absorption energies shown in Table 2 in the main text. Therefore, bulk Cs_4PbBr_6 was not excited in those experiments. It is likely that CsPbBr_3 was excited instead. The thermal quenching of the green emission is not necessarily the result of exciton dissociation. Other mechanisms, e.g., exciton hopping from the CsPbBr_3 inclusion to defects near the $\text{CsPbBr}_3/\text{Cs}_4\text{PbBr}_6$ interface, can also cause thermal quenching of the green emission. Therefore, the exciton binding energy may not be deduced from the temperature-dependent PL measurement.

Analysis of PL intensity versus excitation power in Cs_4PbBr_6 displays a power law dependence for the green emission. The value of the exponential coefficient is 0.7,²² which is below the range (between 1 and 2) that typically corresponds to excitonic emission.¹⁸ Such emission saturation may occur for defect-induced emission when nearly all the defects are excited by high-power excitation; therefore, this behavior can be explained by the CsPbBr_3 inclusions in Cs_4PbBr_6 , which essentially act as defects. Again, this measurement was performed by using excitation [3.06 eV (405 nm)] below the excitonic absorption,²² which can excite CsPbBr_3 but not Cs_4PbBr_6 .

The above analysis strongly supports the view that the green emission observed in Cs_4PbBr_6 is not due to the intrinsic properties of Cs_4PbBr_6 but is rather the result of CsPbBr_3 inclusions embedded within bulk Cs_4PbBr_6 .

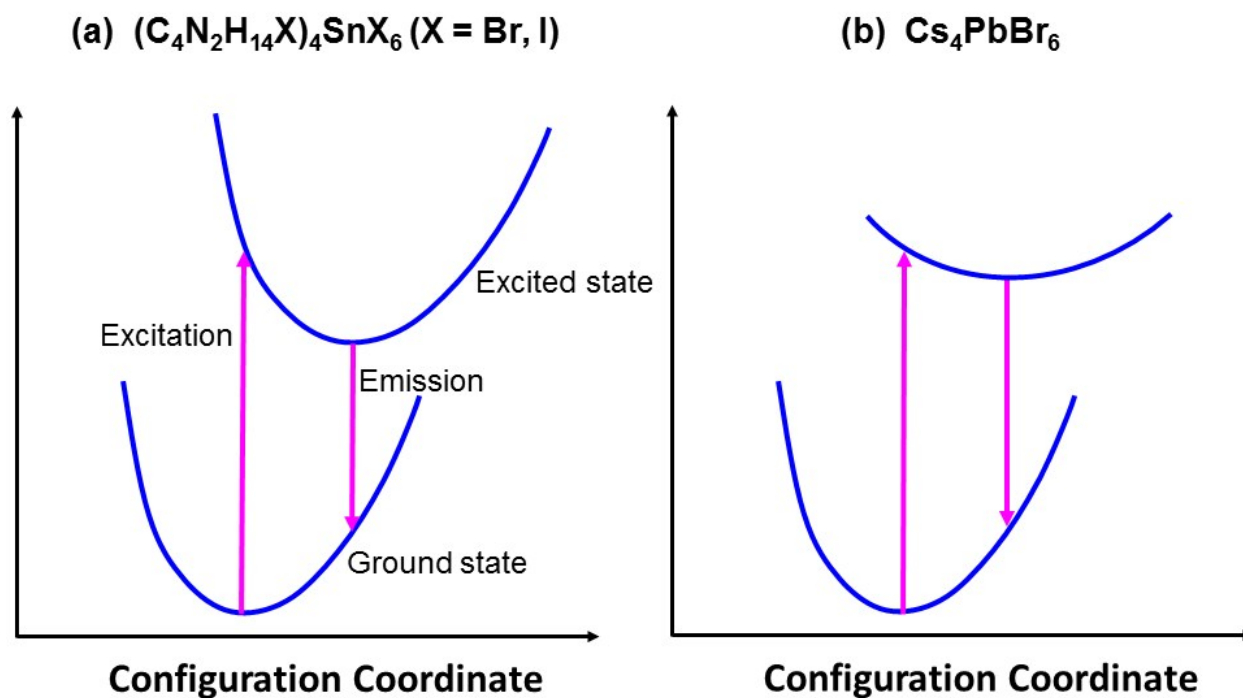


Figure S1. Schematics of exciton excitation and emission in (a) $(C_4N_2H_{14}Br)_4SnX_6$ ($X = Br, I$) and (b) Cs_4PbBr_6 . Note that the excited-state relaxation and the Stokes shift in Cs_4PbBr_6 are relatively small compared to those in $(C_4N_2H_{14}Br)_4SnX_6$ ($X = Br, I$). For simplicity, the intersystem crossing that converts the spin-singlet to the spin-triplet exciton is omitted in the diagram.

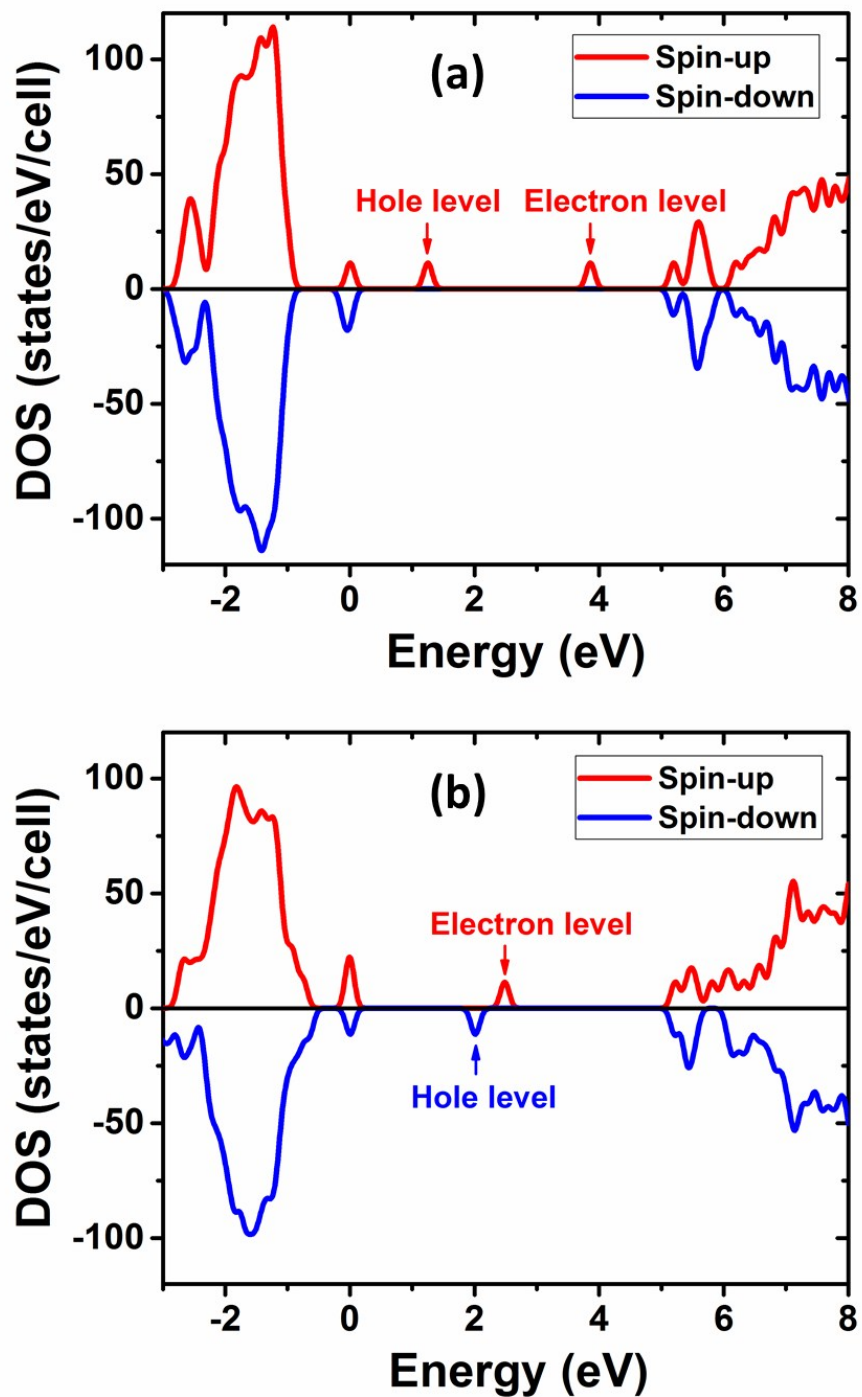


Figure S2. Density of states (DOS) of (a) the unrelaxed spin-singlet exciton and (b) the relaxed spin-triplet exciton in $(\text{C}_4\text{N}_2\text{H}_{14}\text{Br})_4\text{SnBr}_6$, calculated using the PBE0 functional.

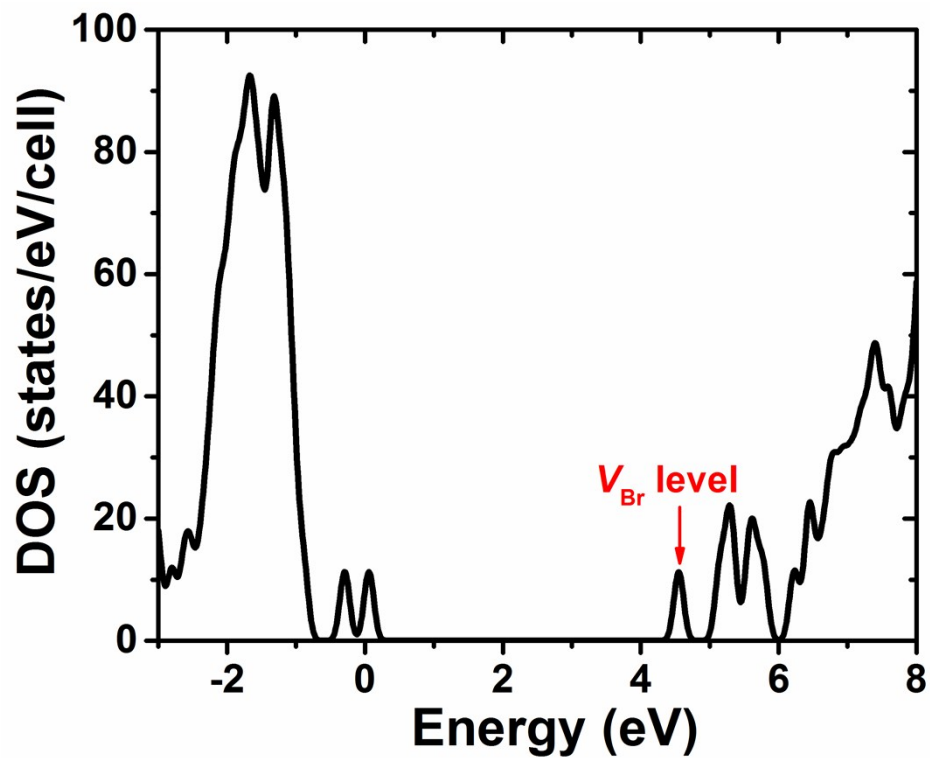


Figure S3. Density of states (DOS) of the V_{Br}^+ -induced level inside the band gap of $(\text{C}_4\text{N}_2\text{H}_{14}\text{Br})_4\text{SnBr}_6$, calculated using the PBE0 functional.

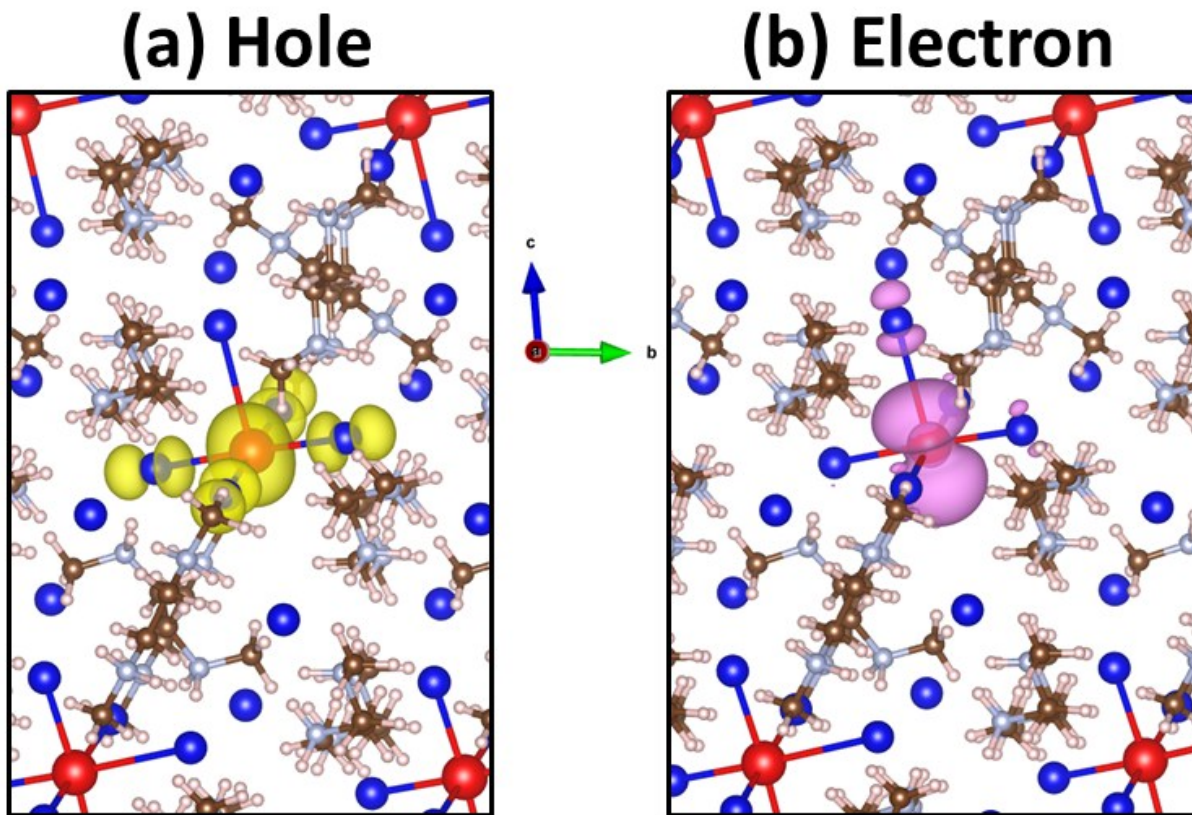


Figure S4. Partial densities of the electron and the hole wavefunctions in the exciton trapped at V_{Br}^+ in $(\text{C}_4\text{N}_2\text{H}_{14}\text{Br})_4\text{SnBr}_6$.

References:

1. G. Kresse and J. Furthmüller, *Computational Materials Science*, 1996, **6**, 15-50.
2. G. Kresse and D. Joubert, *Physical Review B*, 1999, **59**, 1758.
3. C. Zhou, H. Lin, Y. Tian, Z. Yuan, R. J. Clark, B. Chen, B. van de Burgt, J. C. Wang, Y. Zhou, K. Hanson, Q. Meisner, J. Neu, T. Besara, T. Siegrist, E. Lambers, P. I. Djurovich and B. Ma, *Chemical Science*, 2017, DOI: 10.1039/C7SC04539E.
4. M. Velázquez, A. Ferrier, S. Péchev, P. Gravereau, J.-P. Chaminade, X. Portier and R. Moncorgé, *Journal of Crystal Growth*, 2008, **310**, 5458-5463.
5. J. P. Perdew, M. Emzerhof and K. Burke, *Journal of Chemical Physics*, 1996, **105**, 9982-9985.
6. M. Nikl, E. Mihokova, K. Nitsch, F. Somma, C. Giampaolo, G. P. Pazzi, P. Fabeni and S. Zazubovich, *Chemical Physics Letters*, 1999, **306**, 280-284.
7. F. Chiarella, A. Zappettini, F. Licci, I. Borriello, G. Cantele, D. Ninno, A. Cassinese and R. Vaglio, *Physical Review B*, 2008, **77**, 045129.
8. Y. Takahashi, R. Obara, Z.-Z. Lin, Y. Takahashi, T. Naito, T. Inabe, S. Ishibashi and K. Terakura, *Dalton Transactions*, 2011, **40**, 5563-5568.
9. M. Rodová, J. Brožek, K. Knížek and K. Nitsch, *Journal of Thermal Analysis and Calorimetry*, 2003, **71**, 667-673.
10. M.-H. Du and D. J. Singh, *Physical Review B*, 2010, **81**, 144114.
11. M.-H. Du and D. J. Singh, *Physical Review B*, 2010, **82**, 045203.
12. M. H. Du, *Journal of Materials Chemistry A*, 2014, **2**, 9091-9098.
13. D. Chen, Z. Wan, X. Chen, Y. Yuan and J. Zhong, *Journal of Materials Chemistry C*, 2016, **4**, 10646-10653.
14. M. I. Saidaminov, J. Almutlaq, S. Sarmah, I. Dursun, A. A. Zhumekenov, R. Begum, J. Pan, N. Cho, O. F. Mohammed and O. M. Bakr, *ACS Energy Letters*, 2016, **1**, 840-845.
15. S. Seth and A. Samanta, *The Journal of Physical Chemistry Letters*, 2017, **8**, 4461-4467.
16. M. De Bastiani, I. Dursun, Y. Zhang, B. A. Alshankiti, X.-H. Miao, J. Yin, E. Yengel, E. Alarousu, B. Turedi, J. M. Almutlaq, M. I. Saidaminov, S. Mitra, I. Gereige, A. AlSaggaf, Y. Zhu, Y. Han, I. S. Roqan, J.-L. Bredas, O. F. Mohammed and O. M. Bakr, *Chemistry of Materials*, 2017, **29**, 7108-7113.
17. Y. Zhang, M. I. Saidaminov, I. Dursun, H. Yang, B. Murali, E. Alarousu, E. Yengel, B. A. Alshankiti, O. M. Bakr and O. F. Mohammed, *The Journal of Physical Chemistry Letters*, 2017, **8**, 961-965.
18. M. Sebastian, J. A. Peters, C. C. Stoumpos, J. Im, S. S. Kostina, Z. Liu, M. G. Kanatzidis, A. J. Freeman and B. W. Wessels, *Physical Review B*, 2015, **92**, 235210.
19. Q. A. Akkerman, M. Gandini, F. Di Stasio, P. Rastogi, F. Palazon, G. Bertoni, J. M. Ball, M. Prato, A. Petrozza and L. Manna, 2016, **2**, 16194.
20. J.-H. Cha, J. H. Han, W. Yin, C. Park, Y. Park, T. K. Ahn, J. H. Cho and D.-Y. Jung, *The Journal of Physical Chemistry Letters*, 2017, **8**, 565-570.
21. L.-y. Huang and W. R. L. Lambrecht, *Physical Review B*, 2013, **88**, 165203.
22. H. Zhang, Q. Liao, Y. Wu, J. Chen, Q. Gao and H. Fu, *Physical Chemistry Chemical Physics*, 2017, **19**, 29092-29098.